Food Sci. Technol. Res., **14** (3), 221 – 231, 2008

Determination of the Viscoelastic Properties of Apple Flesh under Quasi-Static Compression Based on Finite Element Method Optimization

Gyeong-Won Kim[1*], Man-Soo Kim[2], Yasuyuki Sagara[3], Yeong-Hwan Bae[4], In-Bok Lee[5], Gab-Soo Do[6], Sung-Hyoun Lee[1] and Suk-Won Kang[1]

[1] *National Institute of Agricultural Engineering, Rural Development Administration, 249 Seodun-dong, Gwonson-gu, Suwon, 441-707, Korea*

[2] *Division of Bio-Resources Engineering, Chungnam National University, 220 Gung-dong, Yuseong-gu, Daejeon, 305-764, Korea*

[3] *Department of Global Agricultural Sciences, Graduate School of Agricultural and Life Sciences, University of Tokyo, 1-1-1 Yayoi, Bunkyo-ku, Tokyo, 113-8657, Japan*

[4] *Department of Industrial Machinery Engineering, Sunchon National University, 315 Maegok-dong, Sunchon, 540-742, Korea*

[5] *Department of Bio-Systems Engineering, Seoul National University, San 56-1, Silim-dong, Gwanak-gu, Seoul, 151-742, Korea*

[6] *Department of Bioenvironmental and Agricultural Engineering, College of Bioresource Sciences, Nihon University, 1866 Kameino, Fujisawa-shi, Kanagawa, 252-8510, Japan*

Received August 1, 2007; Accepted January 15, 2008

A procedure for determining the viscoelastic properties of apple flesh has been proposed based on compression tests and FEM optimization. Short-term simple compression tests and long-term relaxation tests were performed with cylindrical specimens of apple flesh to measure mechanical properties, and the viscoelastic behavior was predicted using FEM optimization models. Through short-term optimization, the elastic modulus and Poisson's ratio were determined by comparing two kernel functions based on 1) shear only and 2) shear and bulk terms. Long-term stress-relaxation behavior of the specimen was reasonably predicted by two FEM optimization steps within 3.8 % error. The FEM optimization algorithms developed in this research might be applied to determine the viscoelastic properties of bio-materials and also to predict mechanical behavior of these materials under various loading conditions.

Keywords: apple flesh, compression, stress relaxation, FEM optimization, vicoelastic properties

Introduction

Mechanical properties of fruits and vegetables have been investigated to minimize physical damages such as bruises and scratches during harvest, storage and transportation (Kim *et al.*, 1992). It has been recognized that fruits and vegetables exhibit viscoelastic behavior when subjected to external loading. However, reliable data have rarely been available regarding the viscoelastic properties of fruits due to weak texture and high water contents. For instance, the succulent and weak texture of apple flesh usually prevents researchers from obtaining intact flesh specimens and thus reduces reliability of experimental data (Park, 1993). Extraction of fruit juice during compression tests with flesh specimens imposes an additional problem of mass imbalance since the amount of water loss is not negligible. Therefore, it is difficult to evaluate the physical properties of fruit flesh with sufficient accuracy.

Mechanical properties of viscoelastic materials are usually represented by such factors as elastic modulus, Poisson's ratio, relative elastic modulus, equilibrium elastic modulus and relaxation time. Simple compression experiments using cylindrical specimens are the general procedure to evaluate the stress and strain up to bioyield point (BP) and apparent elastic modulus from force-deformation (F-D) curves, while Poisson's ratio is determined by the relationship between longitudinal and lateral strain (Chappell and Hamann, 1968; Jung, 1999). On the other hand, evaluations of relative elastic modulus, i.e., the quotient of decay elastic modulus and instantaneous elastic modulus, and equilibrium elastic modulus

*To whom correspondence should be addressed.
Email: kim8415@rda.go.kr

require regression modeling of nominal stress-relaxation or creep behavior (Kim and Choi, 1992; Wang, 2003).Usually the geometry of specimen is not included in these models and only long-term deformation is considered.

To overcome the difficulties associated with handling actual fruit specimens, researchers have been utilizing digital simulation techniques based on finite element analysis. Application of finite element method (FEM) enables researchers to evaluate various models and to simulate various boundary conditions notwithstanding the limitation that outcomes rely considerably on the assumed values of fruit texture (Chen and De Baerdemaeker, 1993). FEM applications include nondestructive sensing of the firmness of melon (Chen *et al.*, 1996), modeling of single apple cell (Wu and Pitts, 1999), and analysis of mechanical damage of grape under compressive loading (Rong *et al.*, 2004). Applications of FEM to fruits have been focused mostly on the evaluation of vibration characteristics and estimation of flesh firmness. However, no attempt has been made to evaluate the viscoelastic properties of fruit flesh based on the results of compression and stress-relaxation tests using FEM optimization. The objectives of this research were to determine the viscoelastic properties of apple flesh by simple compression experiments, to develop FEM optimization algorithms to determine related parameters, and to evaluate the validity of FEM optimization results with respect to the predicted regression models.

Materials and Methods

Basic assumptions The following assumptions were made in this research in analyzing the cylindrical specimens of apple flesh:

1. System energy and mass are conserved during compression.
2. Texture of apple flesh is homogeneous and isotropic.
3. Gravity and temperature effects are negligible.
4. No strain hardening of texture occurs during compression.
5. During deformation and loading, Poisson's ratio is held constant and the cylindrical column expands radially and homogeneously.
6. There is no inflection point below the first BP in the F-D curve.

Compression tests Sixty apples ('Fuji') harvested on Sep. 18, 2004 were purchased at a commercial market in Korea for compression tests. After conditioning them for one day at room temperature of 27°C and relative humidity of 60%, sound ones without any defects were selected by visual inspection. The volume, density, and moisture content of the apples averaged 4.01×10^{-4} m^3 , 839.9 kg/m^3, and 84.0%, respectively. A total of 20 cylindrical columns of apple flesh were obtained by extracting central portions of half-cut apples using a 16.6 mm diameter cork borer (Fig. 1). Mechanical damages on apples were commonly found along the equator due to the relative weakness in texture in this area. Therefore, samples were taken by boring the fruits from the cheek (equator) to the central portion of half-cut apples. Each column was cut to a length of 20 mm by using a cutter and a plastic jig. Compression tests were performed for ten cylindrical specimens on Sep. 25, 2004 using a universal testing machine (Stable Microsystems Texture Analyzer, Surry, England) with a flat loading plate of 70 mm in diameter and 10 mm in thickness. To obtain sufficient viscoelastic effect, the test speed was kept at 0.1 mm per second (i.e., a strain rate of 0.005 per second) according to the ASAE standard (ASAE, 2001). Force and deformation data were collected at a rate of 100 points per second.

Relaxation tests were also performed on another set of ten cylindrical specimens according to similar procedures. After applying a strain of 0.05 at a deformation rate of 0.1 mm per second, reaction force was recorded for 600 seconds with the deformation held constant.

Manipulation of F-D curves After determining a BP from an F-D curve, 0.15 BP and 0.5 BP (the points corresponding to 15% and 50% of the force at the BP, respectively) were calculated by linear interpolation (ASAE, 2001). We utilized these three points (0.15 BP, 0.5 BP and BP) from each F-D curve to determine apparent elastic modulus, strain energy, and so forth. In the process of trimming the cylindrical columns, the formation of inclined planes of over 0.1 mm in height at both ends was inevitable, and some broken textures of about 0.05 mm in depth were observed at the trimmed ends and around the column surfaces. To correct the error caused by this inconsistency, we modified the beginning portion of each F-D curve by using a second-order polynomial fit of the F-D data from 0.15 BP to BP. Thus, new starting point for each F-D curve, represented by α in

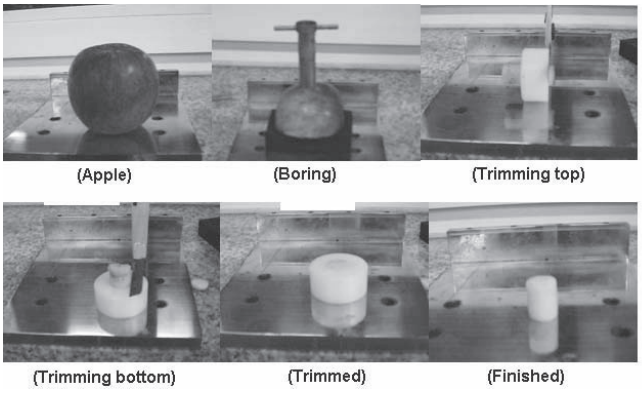

Fig. 1. The procedure of preparing a cylindrical specimen of apple flesh.

Fig. 2, was obtained.

FEM model and governing equations Using ANSYS 8.1 (ANSYS Co., Canonsburg, PA, USA), a commercial FEM program, a hexahedral element model was created to express the viscoelastic properties of apple flesh for small and large deformations. It had three degrees of freedom at each node: translations in the nodal x, y, and z directions. The geometry of this model was a three-dimensional cylinder and made symmetrical to the three axes to save run time (Fig. 3). Every element of this model was meshed to a length of about 1.0 mm.

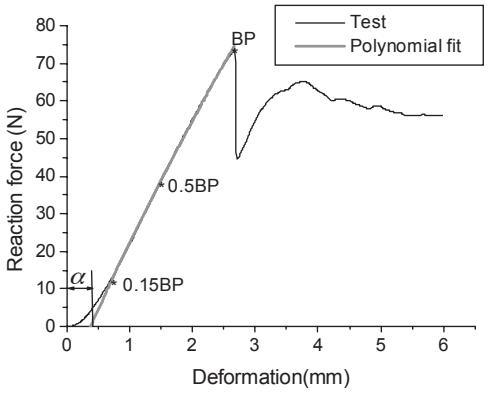

Fig. 2. Second-order polynomial fit from 0.15 BP to BP to determine the amount of horizontal shift α.

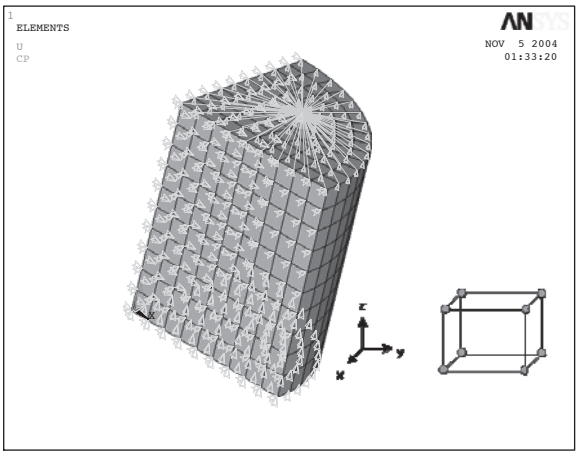

Fig. 3. Mesh geometry for analysis of FEM compression under deformation control.

Using SAS Ver. 8.1 (SAS Institute Inc, Cary, NC, USA) a nonlinear stress-relaxation analysis was conducted by the Marquardt nonlinear regression method for the data obtained from the relaxation tests with ten cylindrical specimens of apple flesh. The results would be utilized as input data to explain the short- and long-term viscoelastic behaviors by FEM optimization and simulation. From the nonlinear regression of the stress relaxation as shown in Fig. 4, the generalized Maxwell model of apple flesh was expressed using equilibrium and decay moduli and relaxation times of Prony series (i.e., a series of the form $\sum_{i=1}^{n} \alpha_i \cdot e^{-t/\tau_i}$ where α_i is the exponential coefficients) with two terms by the following equations (Chen, 2000; Wang, 2003; Ansys, 2000):

$$\sigma(t) = \varepsilon_0[E_e + E_1 \exp(-(t-t_0)/\tau_1) + E_2 \exp(-(t-t_0)/\tau_2)]$$
$$E_0 = E_e + (E_1 + E_2) \quad (1)$$
$$\eta_i = \tau_i E_i \ (i = 1,2)$$

where $\sigma(t)$ and ε_0 are nominal relaxation stress and nominal initial strain, respectively. E_0 and E_e are the instantaneous and equilibrium elastic moduli, respectively. E_1 and E_2 are the first and second decay elastic moduli (Wang, 2003; Ansys, 2000), and τ_1 and τ_2 are the first and second relaxation times of the Prony series, respectively. η_i is the specific viscosity of i-th term. t ($t \geq t_0$) and t_0 are current time and the past time until the beginning of the relaxation, respectively.

Table 1 shows a summary of the nonlinear simulation re-

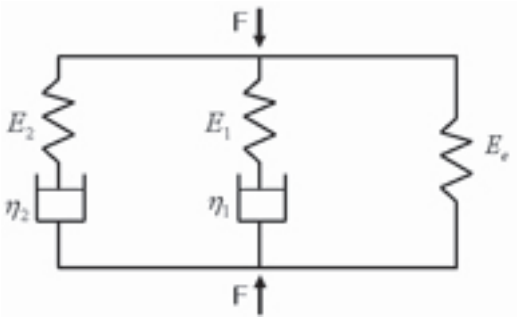

Fig. 4. Regression model for stress relaxation of apple flesh.

Table 1. Summary of Prony series parameters for stress relaxation of the ten apple flesh specimens ($\varepsilon_0 = 0.05$).

Items	$\sigma(t) = \varepsilon_0[E_e + E_1 \exp(-(t-t_0)/\tau_1) + E_2 \exp(-(t-t_0)/\tau_2)]]$								X^2
	E_e (kPa)	E_0 (kPa)	E_1 (kPa)	τ_1 (s)	E_2 (kPa)	τ_2 (s)	$\frac{E_1}{E_0}$	$\frac{E_2}{E_0}$	(×10^{-3})
Max.	1315.7	2316.1	546.6	275.7	453.8	25.7	0.279	0.196	1.1
Min.	660.1	1186.5	330.5	138.7	195.9	12.4	0.236	0.145	0.08
Ave.	1005.5	1732.4	428.5	186.9	298.3	17.0	0.252	0.169	0.19
STDEV	329.2	565.8	109.4	77.0	136.9	7.5	0.023	0.026	0.24

X^2 indicates an error function, which was used as an objective function of nonlinear regression (SAS8.1, 2001).

sults of the generalized Maxwell model. The averages of the relaxation time and the quotient of decay elastic modulus and instantaneous elastic modulus of the first Prony series term were 186.9 s and 0.252, respectively. Also, those of the second term were 17 s and 0.169, respectively. Therefore, the two specific viscosities (η_1 and η_2), calculated by Eq. (1), resulted in 80.08 and 5.07 MPa·s, respectively.

It was assumed that the quotient of decay modulus and instantaneous modulus for each term of Prony series was held constant for elastic, shear, and bulk modulus components as follows:

$$\beta_i^E = \frac{E_i}{E_0} = \beta_i^G = \frac{G_i}{G_0} = \beta_i^K = \frac{K_i}{K_0} \quad (i = 1,2) \tag{2}$$

where β_i^E, β_i^G, and β_i^K indicate relative decay moduli for Young's, shear, and bulk in relaxation, respectively, for the i-th term of the Prony series. Also, G_i and K_i are the i-th term of decay shear modulus and decay bulk modulus, respectively. Utilizing the results of nonlinear regression analysis of the stress-relaxation behavior, the following two kernel functions were proposed:

$$G(t) = G_0\left[\beta_\infty^G + \sum_{i=1}^{nG} \beta_i^G \exp(-t/\tau_i^G)\right] \tag{3}$$

$$K(t) = K_0\left[\beta_\infty^K + \sum_{i=1}^{nK} \beta_i^K \exp(-t/\tau_i^K)\right] \tag{4}$$

where $G(t)$ is the kernel function for shear relaxation and $K(t)$ is for bulk relaxation. To compare the functional ability in convergence and determination of viscoelastic properties of apple flesh for short- and long-term FEM simulations, two optimization schemes were applied: one with shear modulus only and the other with shear and bulk moduli. Followings are two kernel functions based on hereditary integration for FEM Cauchy stress:

FEM optimization using shear function only,

$$\sigma = \int_0^t 2G(t-\xi)\frac{de}{d\tau}d\tau \tag{5}$$

FEM optimization using shear+bulk function,

$$\sigma = \int_0^t 2G(t-\xi)\frac{de}{d\tau}d\tau + I\int_0^t K(t-\xi)\frac{d\Delta}{d\tau}d\tau \tag{6}$$

where σ and I are the Cauchy stress and unit tensor, respectively; ξ is past time; and e and Δ indicate deviatory strain and volumetric strain, respectively.

FEM optimization and evaluation To make mechanical FEM behaviors of apple flesh resemble those of real compression experiments, the FEM boundary conditions as well as physical element geometry of the model were considered important in all aspects of optimization loop in determining the viscoelastic properties. Viscoelastic properties such as elastic modulus (E) and Poisson's ratio (ν); and relaxation properties such as shear and bulk relative moduli (β^G, β^K), relaxation time (τ)and equilibrium and decay elastic moduli (E_e, E_i) were obtained by using Sequential Unconstrained Minimization Technique (SUMT) algorithm supported by the ANSYS program. In this SUMT algorithm of FEM optimization the dependent variables (state variables and objective function) with independent design variables are first represented by approximation (Eq. (7) and Eq. (8), respectively) with fully quadratic cross terms of design variables in Eq. (9) and accomplished by means of least squares fitting in Eq. (10):

$$\hat{g}(x) = g(x) + error \tag{7}$$

$$\hat{f}(x) = f(x) + error \tag{8}$$

$$\hat{f} = a_0 + \sum_i^n a_i x_i + \sum_i^n \sum_j^n b_{ij} x_i x_j \tag{9}$$

$$error^2 = \sum_{j=1}^{n_d} (f^{(j)} - \hat{f}^{(j)})^2 \tag{10}$$

were a_0, a_i, and b_{ij} are constants for quadratic representation with cross terms.

Finally SUMT algorithm is used to solve Eq. (11) for each design iteration at which the constrained minimization problem is converted to an unconstrained problem using penalty functions:

$$F(x, p_k) = \hat{f} + f_0 p_k \left(\sum_{i=1}^{n} X(x_i) + \sum_{i=1}^{m_1} G(\hat{g}_i)\right) \tag{11}$$

where $F(x, P_k)$ is an unconstrained objective function and x is the penalty function used to enforce design variable constraints; and f_0 is introduced in order to achieve consistency in the units. P_k is a response surface parameter and G is penalty function for state variable constraints.

Fig. 5 shows the optimization procedure utilized in this research and the boundary conditions are summarized in Table 2. Prior to FEM optimization, FEM simulation was carried out to check geometry conditions such as constrains and element size as mentioned in Fig. 3 and to judge the initial values of parameters as suitable ones

All FEM optimization and simulation analyses were transient and controlled by the displacement. Two optimization steps were utilized in this algorithm. The first step compared functional ability between the two kernel functions (shear and shear+bulk) in determining two design variables (E and ν) for ten specimens of apple flesh. In this step, the objective function was aimed to minimize the difference of work be-

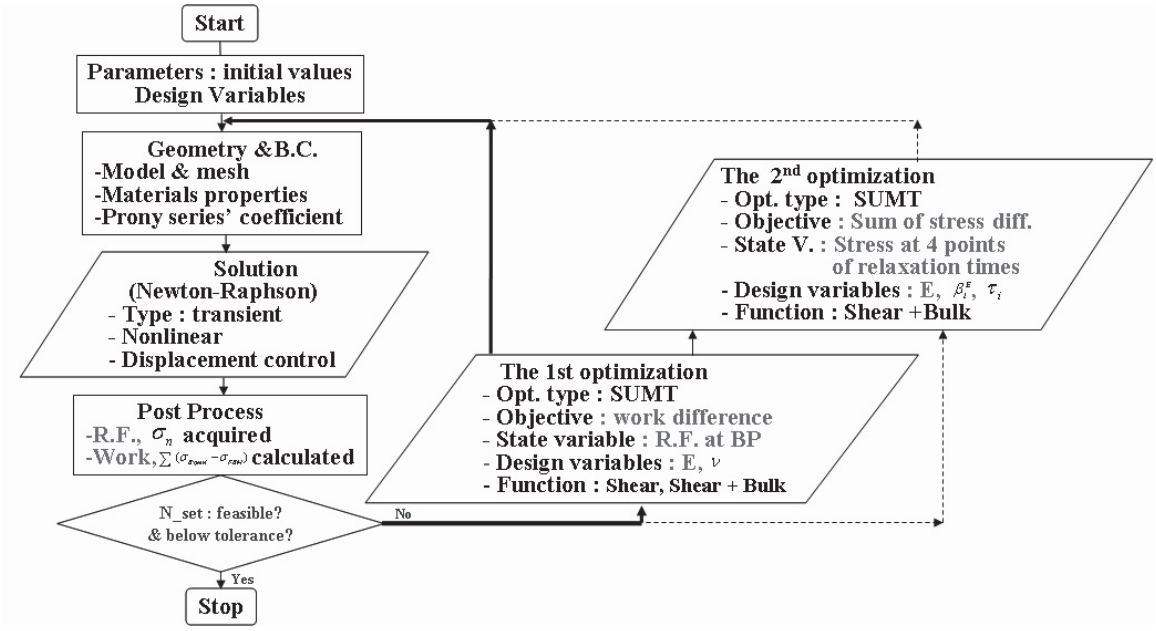

Fig. 5. Flow chart of FEM optimization for apple flesh.

Table 2. The boundary conditions for objective function, state variable, and design variables.

Items			Initial values	Bounds	Tolerance
Objective function	1st Opt.		—	—	0.01
	2nd Opt.		—	—	
State variables	1st Opt.		—	99% value of experiment	0.01
	2nd Opt.		—		
Design variables	1st Opt.	E	2.71 MPa	0.2≤E≤5.0	0.001
		ν	0.27	0.25≤ν≤0.4	
	2nd Opt.	E	Result of 1st Opt.	Initial ± 50%	0.001
		β_i^E	Values of nonlinear regression	β_i^E: 0.1 to 1.0	0.01
		τ_i		τ_i : 1 to 1000 (s)	

tween compression experiments and FEM up to BP of each F-D curve. The difference in reaction force between the experiments and FEM was used as a state variable and its value was maintained below 2% at 0.5BP and 1% at BP for enforcing convergence during FEM optimization. The bounds for the design variables (E and ν) were adapted from literature (De Baerdemaeker and Segerlind, 1976; Chappell and Hamann, 1968; Jung, 1999; Kim et al., 1992; Park, 1993). One specimen (A1) was used to determine the suitable optimization procedure that allowed stabilization of the FEM algorithm. With the optimization results derived from the first step of the A1 specimen, three types of FEM simulations, i.e. two for viscoelastic functions composed of shear and shear+bulk kernel functions and the other for elastic function, were carried out to compare their reaction forces at BP according to the variation of Poisson's ratio from 0.2 to 0.48 with fixing the other constants of shear+bulk optimization result. These simulations also demonstrated the mechanical behavior of visco- and nonvisco-elastic properties of apple flesh under the same condition. And also using specimen A1 and kernel function of shear+bulk, to assure the hydrostatic pressure on the cylindrical specimen of apple flesh, Von Mises stress expressed in Eq. (12) and Eq.(13) was checked at the time point of 0.58 s (initial), 11.55 s (0.5BP), and 23.1 s (BP). The Von Mises theory (Walter, 1994), also called Maxwell-Huber-Hencky-Von Mises theory, states that failure takes place when the principal stress of σ_1, σ_2, σ_3 are such that $2\sigma^2_{yielding} = (\sigma_1-\sigma_2)^2+(\sigma_2-\sigma_3)^2+(\sigma_1-\sigma_3)^2$ The Von Mises stress, σ_{eqv}, is often referred to as the equivalent stress and available output of general purpose in structural analysis (ANSYS, 2004):

$$\sigma_{eqv} = \left[\frac{(\sigma_1-\sigma_2)^2+(\sigma_2-\sigma_3)^2+(\sigma_1-\sigma_3)^2}{2}\right]^{1/2} \quad (12)$$

or

$$\sigma_{eqv} = \left[\frac{(\sigma_x-\sigma_y)^2+(\sigma_y-\sigma_z)^2+(\sigma_z-\sigma_x)^2+6(\sigma_{zy}^2+\sigma_{yz}^2+\sigma_{xz}^2)}{2}\right]^{1/2} \quad (13)$$

To expand the validity of the mechanical properties of apple flesh optimized for short-to long-period mechanical behavior, and also to assess the two kernel functions, the FEM simulations of stress relaxation were carried out for the two optimization results: one for kernel function of shear and the other for kernel function of shear+bulk, using the average of the optimized curves for ten specimens at BP. The initial strain of FEM relaxation simulations was 0.118 and the simulation condition was also the same as that of relaxation experiment. The nominal stress of the two FEM-relaxation simulations was compared with that of the nonlinear regression simulation at time points of 50 s, 300 s and 600 s. The nonlinear regression model at that strain was made from nominal stress of kernel function of shear+bulk at BP and using Eq. (1) from which the decay modulus (E_i) and equilibrium elastic modulus (E_e) were calculated. To reduce the difference in long- and short-term mechanical behaviors between FEM simulation and nonlinear regression model, the second optimization step was carried out using the best results of the two functions in the first optimization step. The second step utilized two objective functions expressed in summation of nominal-stress differences between the nonlinear regression and the FEM checked at four time points (initial (23.1 s), 50 s, 300 s, and 600 s) regarding weightless ($w_i=1$, $i=1, 2, 3, 4$) and weight ($w_1=3$, $w_2=w_3=w_4=1$) factor at initial point of time in Eq. (15).

Objective function for the first optimization:

$$\text{W\_diff.} = \left| \int_{x=0}^{x=BP} \left[a + b(x+\alpha) + c(x+\alpha) \right] dx - \int_{x=0}^{x=BP} F_{FEM} dx \right| \quad (14)$$

Objective function for the second optimization:

$$\text{Stress\_diff.} = \left| \sum_{i=1}^{4} w_i \sigma_{\text{Reg}_i} - \sum_{i=1}^{4} w_i \sigma_{FEM_i} \right| \quad (15)$$

where FFEM is reaction force obtained during FEM optimization loop, and σ_{Reg} and σ_{FEM} are nominal stresses of nonlinear regression model and FEM, respectively.

Results and Discussion

Compression tests and manipulation of F-D curves Compression tests with cylindrical specimens of apple flesh under constant strain rate control resulted in the reaction force of 47.85 to 80.60 N and deformation of 2.04 to 3.46 mm at BP. The average reaction force was 61.98 N and average deformation was 2.82 mm, while the average deformations at 0.15 BP (9.30 N) and 0.5 BP (30.99 N) were 0.74 and 1.52 mm, respectively. Nominal stress, that is a reaction force divided by the cross-sectional area of specimen, at BP ranged from 372.6 kPa to 221.2 kPa. The average works per unit volume integrated from the initial strain to 0.15 BP, 0.5 BP, and BP were 0.53 kJ/m^3, 4.23 kJ/m^3, and 18.57 kJ/m^3, respectively. The average apparent elastic moduli at 0.15 BP, 0.5 BP, and BP were 1.220 MPa, 1.917 MPa, and 2.064 MPa, respectively. The apparent elastic modulus increased nonlinearly with the increase in deformation. It rapidly rose by 57.1% in the deformation range from 0.15 BP to 0.5 BP and formed a gentle positive slope with maximum variation of 7.6% from 0.5 BP to BP. These results could be mainly caused not by strain hardening with increased deformation but by point-to-surface contact rather than surface-to-surface contact, which was caused by the inaccurate geometrical shape of cylindrical specimen and the broken structures on the plane surfaces at both ends. These problems were unavoidable when preparing the cylindrical specimen using a cork borer and a knife because of the succulent and weak texture of apple flesh. Thus, abnormalities appeared in the initial strain range of the F-D curves for all specimens: initial convex-downward curve followed by sharply increasing reaction force from the initial deformation to 0.15 BP. The results of the second-order polynomial fitting of the original F-D curve in the range from 0.15 BP to BP were listed in Table 3.

The results showing positive first-order coefficients and negative second-order coefficients indicate that all the curves within the range from 0.15 BP to BP have concave-

Table 3. Results of polynomial fitting F-D curves from 0.15 BP to BP under constant strain-rate compression test.

Specimen	$y = a + b(x+\alpha) + c(x+\alpha)^2$				R^2
	a	b	c	α (mm)	
A1	-14.0480	37.8709	-1.7524	0.3775	0.9997
A2	-10.9491	30.1728	-1.0596	0.3676	0.9994
A3	-16.9295	30.3660	-1.6968	0.5761	0.9997
A4	-13.8347	48.5933	-4.8209	0.2932	0.9999
A5	-8.3654	27.1649	-1.3487	0.3128	0.9997
A6	-4.8889	23.2936	-0.5772	0.2110	0.9997
A7	-13.0812	32.1276	-1.1802	0.4134	0.9993
A8	-17.1953	36.2069	-3.6086	0.4998	0.9992
A9	-21.8762	34.3109	-3.5204	0.6859	0.9993
A10	-27.7950	35.2230	-0.9561	0.8068	0.9996
Average	—	—	—	0.45	0.9995

downward shape similar to that for general polymer materials. The values of α (horizontal shift of F-D curve) ranged from 0.2100 to 0.8068 mm with an average of 0.4500 mm. By adjusting the starting points of F-D curves by α, the average deformation at 0.15 BP, 0.5 BP, and BP were reduced to 0.31 mm, 1.06 mm, and 2.31 mm, respectively. The average works per unit volume at 0.15 BP, 0.5 BP, and BP after modifying the F-D curves were 0.34 kJ/m^3, 4.03 kJ/m^3, and 17.86 kJ/m^3, respectively. Modification of the F-D curves decreased work per unit volume at 0.15 BP, 0.5 BP, and BP by 35.3%, 4.8%, and 3.8% from the original values, respectively. Even though the differences in work per unit volume between before and after the modification of F-D curves did not approach zero, the values at BP and 0.5 BP were considered small. Average values of apparent elastic modulus at 0.15 BP, 0.5 BP, and BP were 2.874 MPa, 2.744 MPa, and 2.522 MPa, respectively, indicating that there was a smooth decrease in the apparent elastic modulus with an increase in deformation, quite opposite to the variation shown in the raw F-D curves(Table 4).

Short-term FEM optimization Fig. 6 shows the convergence of the FEM optimization process for A1 specimen according to the objective function (a), state variable (b), and design variables (c and d). Indicated in the figure are two feasible sets out of ten design sets in case of the kernel function utilizing shear modulus only, and four out of eight in case of shear+bulk kernel. The elastic modulus in the FEM optimization using shear only and shear+bulk converged successfully to 2.776 MPa and 2.805 MPa, respectively, resulting in reductions by -7.8 % and -6.8 % when compared to the value of apparent elastic modulus obtained by the compression test. Poisson's ratio in the two kernel functions (shear and

Table 4. Apparent elastic moduli (E_{App}) at 0.15 BP, 0.5 BP, and BP after modifying the F-D curves (MPa).

Sample	0.15 BP	0.5 BP	BP
Max.	4.135	3.891	3.467
Min.	2.110	2.059	1.98
Average	2.874	2.744	2.522
STDEV	0.562	0.525	0.484

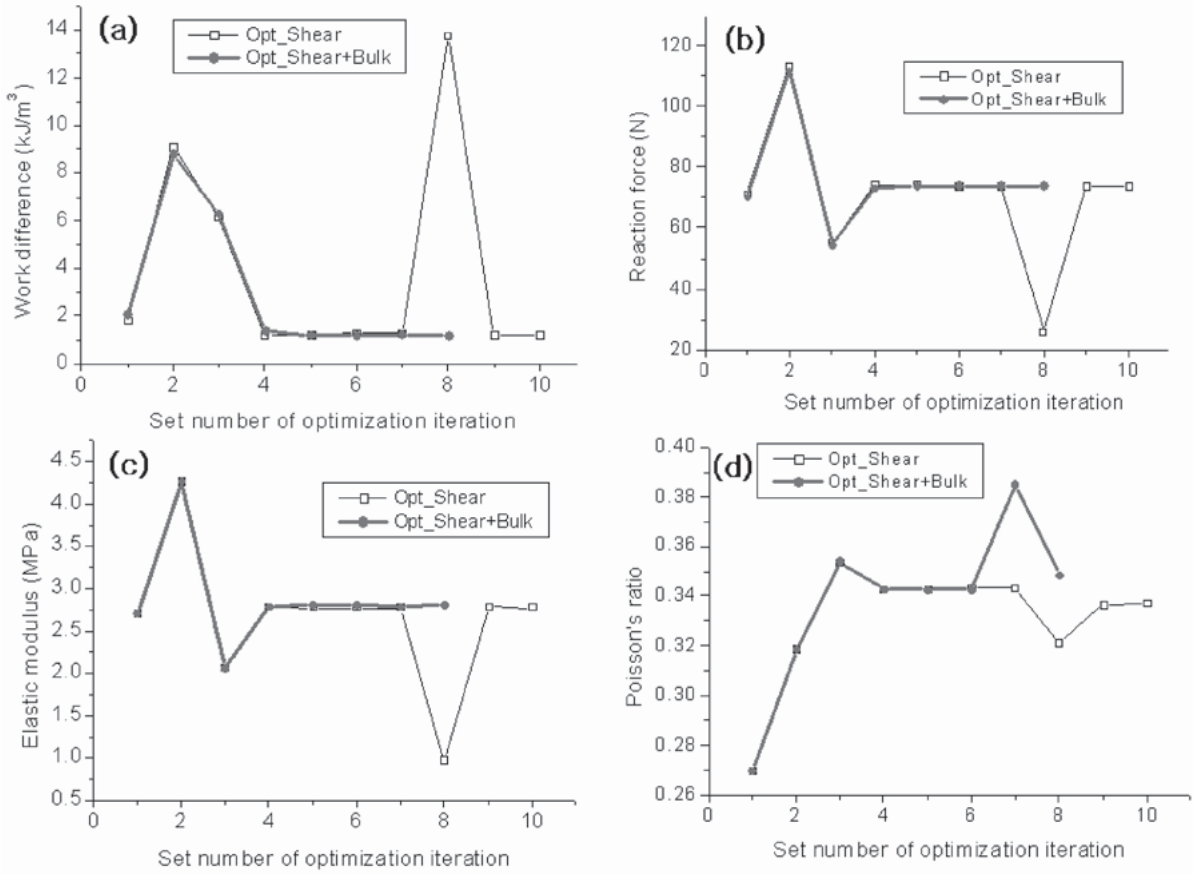

Fig. 6. Comparison of the results of FEM optimization according to kernel functions (shear and shear+bulk): (a) objective function, (b) state variable, (c) elastic modulus, and (d) Poisson's ratio.

shear+bulk) also converged to 0.337 and 0.348, with slight fluctuation shown in the feasible sets in the range from 0.343 to 0.383 while satisfying all constraints. The work differences between the results of FEM and experiments for shear and shear+bulk cases were -5.99 % and -5.70 %, respectively. Moreover, the state valuable (the reaction force at BP) was maintained during the optimization process very stably at 99.9% of the value obtained from the modified F-D curve (78.87 N). From the result of FEM optimization using A1 specimen, no significant difference was found between the two kernel functions considering convergence, state variable, and design valuables.

Fig. 7 shows the effect of Poisson's ratio on the reaction force at BP (strain = 0.116) for specimen A1 according to the type of kernel functions. When Poisson's ratio was 0.348, the reaction forces were 74.77 N for shear model and 73.86 N for shear+bulk model, reduced significantly (by 8.15% and 8.89%, respectively) comparing to the reaction force for elastic model. As Poisson's ratio increased from 0.3 to 0.4, a range covering the Poisson's ratio of apples from various literatures, the changes in reaction forces were 2.50%, 1.69%, and 2.49% for elastic, shear, and shear+bulk models, respectively. The slope of reaction force versus Poisson's ratio was smaller in case of shear model than the other two models. It can be suggested from the figure that the choice of kernel function (elastic or viscoelastic) would have greater effect on the reaction force than the exactness of Poisson's ratio in the range from 0.3 to 0.4.

Finally, full-scale optimization for 10 specimens at BP was successfully completed using the two kernel functions of shear and shear+bulk. Work differences between the average values of the experiment and the FEM for shear and shear+bulk models converged well and resulted in the values of -7.09 % and -6.69 %, respectively, which were considered to be acceptable in general (Table 5). Also, those of reaction force between them were -0.01% and -0.11%, respectively

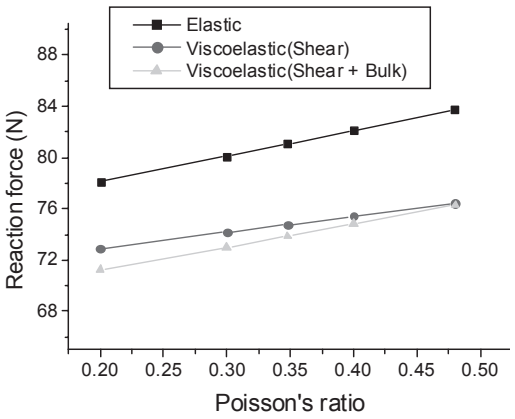

Fig. 7. Relationship between reaction force and Poisson's ratio for three types FEM simulations using A1 specimen at strain of 0.116.

Table 5. Results of reaction force at BP for 10 cylindrical specimens of apple flesh optimized with using two types of kernel functions: shear in Prony series and shear+bulk.

Sample	Shear in Prony series		Shear + Bulk in Prony series	
	FEM R.F. (N)	R.F. difference (%) $\frac{(FEM-Experi.)\times 100}{FEM}$	FEM R.F. (N)	R.F. difference (%) $\frac{(FEM-Experi.)\times 100}{FEM}$
A1	73.86	-0.01	73.86	-0.01
Average	61.98	-0.01	61.92	-0.11
STDEV	10.08	0.01	10.12	0.31

Table 6. Results of work at BP for 10 cylindrical specimens of apple flesh optimized with using two types of kernel functions: shear in Prony series and shear+bulk.

Sample	Shear in Prony series		Shear + Bulk in Prony series	
	FEM Work (kJ/m³)	Work diff. $\frac{(FEM-Experi.)\times 100}{FEM}$ (%)	FEM Work (kJ/m³)	Work diff. $\frac{(FEM-Experi.)\times 100}{FEM}$ (%)
A1	19.30	-5.99	19.36	-5.70
Average	16.65	-7.09	16.67	-6.69
STDEV	4.21	2.48	4.25	-0.25

Table 7. Results of design valuables (elastic modulus, Poisson's ratio) at BP for 10 cylindrical specimens of apple flesh optimized with using two types of kernel functions: shear in Prony series and shear+bulk.

Sample	Shear in Prony series			Shear + Bulk in Prony series		
	E (MPa)	Difference $\frac{(E-E_{app})}{E_{App}}\times 100$ (%)	ν	E (MPa)	Difference $\frac{(E-E_{app})}{E_{App}}\times 100$ (%)	ν
A1	2.776	-7.825	0.337	2.805	-6.859	0.348
Average	2.327	-7.840	0.302	2.343	-7.378	0.333
STDEV	0.466	1.452	0.032	0.499	2.196	0.055

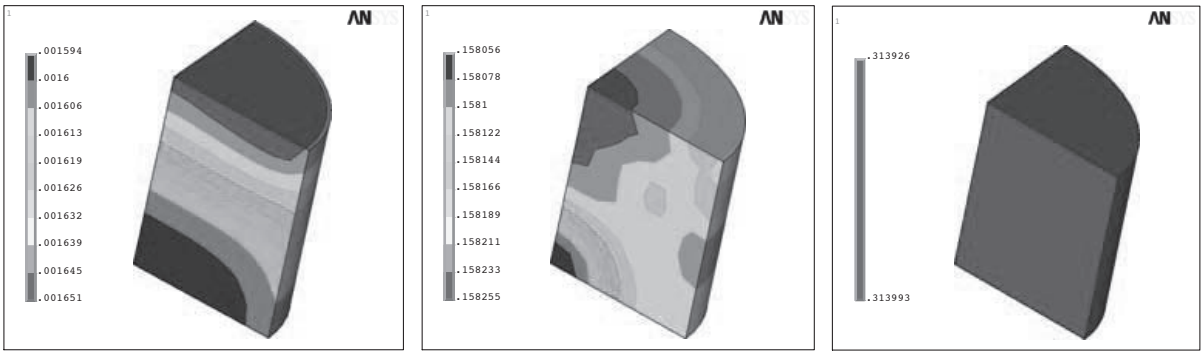

Fig. 8. Von Mises stress contours at 0.58 s (Left), 11.5 s, and 23.1 s (BP) for specimen A1 optimized by the kernel function of shear+bulk.

Table 8. Results of Von Mises stress (σ_{eqv}) at BP for 10 cylindrical specimens of apple flesh optimized with using two types of kernel functions: shear in Prony series and shear+bulk.

Sample	Shear in Prony series		Shear + Bulk in Prony series	
	σ_{eqv} (kPa)	Difference $\frac{\sigma_{eqv}-\sigma_n}{\sigma_n}\times 100$ (%)	σ_{eqv} (kPa)	Difference $\frac{\sigma_{eqv}-\sigma_n}{\sigma_n}\times 100$ (%)
A1	313.8	-8.0	314.0	-8.0
Average	264.9	-7.5	263.4	-8.1
STDEV	42.0	1.3	44.4	2.1

(Table 6). As shown in Table 7, average elastic moduli for the shear and shear+bulk models were 2.327 MPa and 2.33 MPa, respectively, and the average Poisson's ratios were 0.302 and 0.333. The differences in elastic modulus between apparent modulus and the FEM for the shear and shear+bulk models were -7.8 % and -7.4 %, respectively. However, no significant difference was observed in the design variables determined by FEM optimization using two kernel functions (shear and shear+bulk).

As shown in Fig. 8, Von Mises stress at time points of 0.58 s (initial) and 11.55 s (0.5BP) appeared in quite narrow ranges of 1.59 to 1.65 kPa and 158.0 to 158.2 kPa, respectively, but the stress at 23.1 s (BP) was fully hydrostatic with the value of 314.0 kPa. This indicated that fully-developed hydrostatic behavior did not occur at the beginning of load application, presumably due to viscoelastic effect in transient analysis of FEM. As shown in Table 8, the average Von Mises stress of the shear and shear+bulk functions resulted in very close values of 264.9 kPa and 263.4 kPa, respectively. However, these values were lower by as much as 7.5 % for shear function and by 8.1 % for shear+bulk kernel when compared to the apparent modulus of the modified F-D curves.

Evaluation of long-term compression and FEM optimization In applying the results of short-term FEM optimization to long-term stress-relaxation behavior, it was assumed that the relative modulus (β_i) values would not be changed in the strain range of 0.05 to 0.118. The model expression of

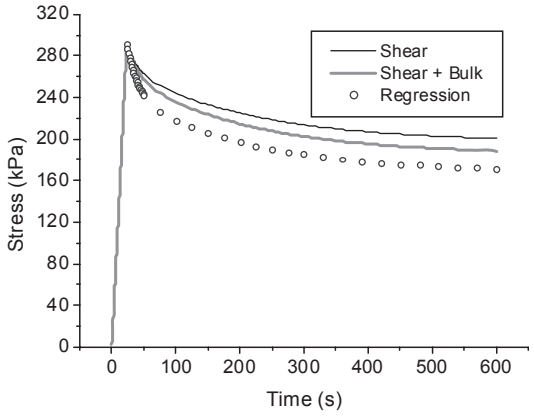

Fig. 9. Comparison of stress relaxation of FEM simulations using two types of optimizations results (Shear and Shear + Bulk) with nonlinear regression at the initial strain of 0.118.

Eq. 1 at the strain of 0.05 was modified (remodeled) and the equilibrium elastic modulus (E_e) and decay elastic modulus (E_i) values obtained by the first step FEM optimization using shear+bulk kernel function was substituted with FEM nominal stress of 291.1 kPa at the initial strain of 0.118 into the equation such that:

$$\sigma(t) = 0.118\,[1{,}428.0 + 622.0\exp(-(t - 23.1)/186.9) + 417.0\exp(-(t - 23.1)/17.0)] \quad (16)$$

where the parameters corresponds to E_e = 1,428.0 kPa, E_1 = 622.0 kPa, E_2 = 417.0 kPa, η_1 = 116.2 MPa·s, and η_2 = 7.1 MPa·s.

Table 9. Results of total stress difference and five design variables from the second optimization for two types (optimization with non-weight factor and with weight factor of 3.0 at initial stress in objective function).

Item	Elastic modulus (MPa) E	relaxation time (s)		Relative modulus of elasticity		Stress difference (kPa) $\sum (\sigma_{Reg.} - \sigma_{FEM})$
		τ_1	τ_2	β_1^E	β_2^E	
2nd Opt.	2.366	170.1	12	0.269	0.212	16.6
2nd Opt. weighted	2.366	170.2	18.2	0.269	0.213	2.9
Initial value	2.343	186.9	17	0.252	0.169	—

Fig. 9 shows the predicted stress by the first long-term FEM optimization. The shear+bulk model is closer to the regression function than the shear only model.

However, the differences in stresses at the four designated time points ranged from 6.2% to 9.8% in case of the shear+bulk model.

The results of the second optimization using the two objective functions (weightless and weighted) and the kernel function of shear+bulk are listed in Table 9.

The optimized design variables of E, β_1^E, β_2^E, τ_1, and τ_2 for weighted objective function were 2.366 MPa, 0.269, 0.213, 170.2 s, and 18.2 s, respectively. The differences in the optimized values of design variables were very small when comparing the results of weightless and weighted objective functions. However, the resulting value of objective function (stress difference) was reduced to one-fifth by adding appropriate weights in the objective function. The predicted stress by the second long-term FEM optimization is shown in Fig. 10. The reduction in prediction error is noticeable when comparing this with the results of Fig. 9. In case of utilizing weighted objective function, the prediction error in nominal stress was less than 3.8% until 50 s and below 1.5% thereafter. The prediction error was 3.8 times higher in case of weightless objective function until 50 s than that of weighted case.

Consequently, the short-term optimization using shear+bulk model provided reasonable predictions of E and ν for apple flesh specimen within 8.0 % prediction error. By adding the second optimization, the long-term mechanical behavior of stress-relaxation was more closely predicted within 3.8 % error. Therefore, the two step optimization scheme was suggested to determine the viscoelastic properties of apple flesh such as E, β_1^E, β_2^E, τ_1, and τ_2. Also the weighted function approach is applied to device the objective function for the second optimization. The values of the viscoelastic properties found in this research (ν of 0.333 from short-term optimization; and E, β_1^E, β_2^E, τ_1, and τ_2 of 2.366 MPa, 0.269, 0.213, 170.2 s, and 18.2 s, respectively, from long-term optimization), corresponded well with the values reported in the literatures (Jung, 1999; Kim *et al.*, 1992; Park, 1993). The FEM optimization algorithms developed in this research might be applied to determine the viscoelastic properties of bio-materials and also to predict mechanical behavior of these materials under various loading conditions.

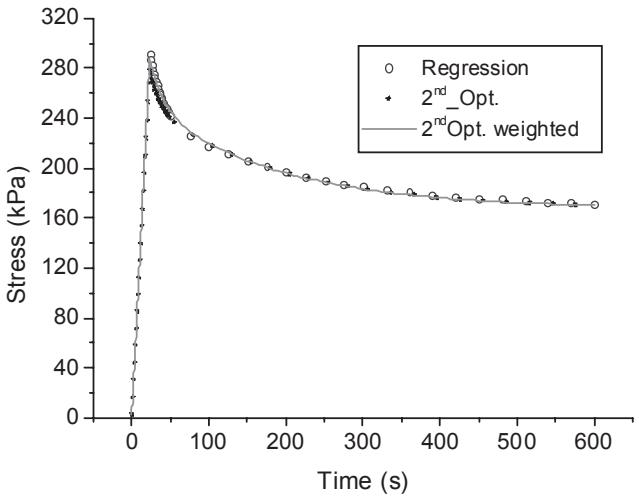

Fig. 10. Comparison of nominal stress of two FEM simulations (the objective having weight factor and weightless factor) with that of nonlinear regression at initial strain of 0.118 relaxed for 600 seconds.

References

Anand, A. and Scanlon, M.G. (2002). Dimensional effects on the prediction of texture-related mechanical properties of foods by indentation. *Trans. of the ASAE*, **45**, 1045-1050.

ANSYS. (2004). Elements, theory, and optimization. User's Manual, Version 8.1, Canonsburg, PA.

ASAE. (2001). Compression test of food materials of convex shape. In "ASAE Standards", ASAE S368.4, St. Joseph, MI, pp. 580-587.

Chappell, T.W. and Hamann, D.D. (1968). Poisson's ratio and Young's modulus for apple flesh under compressive loading. *Trans. of the ASAE*, **15**, 608-610, 612.

Chen, H. and De Baerdemaeker, J. (1993). Finite-element-based model analysis of fruit firmness. *Trans. of the ASAE*, **36**, 1827-1833.

Chen, H., De Baerdemaeker, J.G. and Bellon, V. (1996). Finite ele-

ment study of the melon for nondestructive sensing of firmness. *Trans. of the ASAE*, **39**, 1057-1065.

Chen, T. (2000). Determining a Prony series for a viscoelastic material from time varying strain data. NASA TM-210123, Hampton, VA.

De Baerdemaeker, J.G. and Segerlind, L.J. (1976). Determination of the viscoelastic properties of apple flesh. *Trans. of the ASAE*, **17**, 346-348, 353.

Jung, H.M. (1999). Mechanical properties of selected fruits and vegetables. M.Sc. Thesis, Chungnam National University, Daejeon, Korea (in Korean).

Kim, M.S., Park, J. M. and Choi, D. S. (1992). Viscoelastic properties of fruit flesh (1) - Stress relaxation behavior. *J. Kor. Soc. Agric. Mach*, **17**, 260-271 (in Korean).

Rong, W., Qunying J. and Deqiang, W. (2004). On the mechanical damage of grape using finite element analysis. ASAE Paper 046190, St. Joseph, MI.

Park, J.M. (1993). Viscoelastic properties of fruits and their applications. Ph.D. Dissertation, Chungnam National University, Daejeon, Korea (in Korean).

SAS (2001). The nonlinear procedure, SAS Online Document, Version 8.1, www.sashelp.sline21.net.

Walter D (1994). Formulars for stress, strain, and structural matrices. John Wiley & Sons, Inc., pp. 130-131.

Wang J. (2003). Anisotropic relaxation properties of pear. Biosystems Engineering, **85**, 59-65.

Wu, N. and Pitts, M.J. (1999). Development and validation of a finite element model of an apple fruit cell. *Postharvest Biology and Technology*, **16**, 1-8.